On the Sensing Mechanisms of a Hydroresistive Flexible Film based on an Organic Molecular Metal

Raphael Pfattner,[1,2] Elena Laukhina,[2,*] Laura Ferlauto,[3,†] Fabiola Liscio,[3] Silvia Milita,[3] Anna Crespi,[1] Victor Lebedev,[1,2] Marta Mas-Torrent,[1,2] Vladimir Laukhin,[1,2,4] Concepció Rovira[1,2] and Jaume Veciana[1,2,*]*

1) *Institut de Ciència de Materials de Barcelona (ICMAB-CSIC) Campus UAB, 08193 Bellaterra, Spain*

2) *Networking Research Center on Bioengineering Biomaterials and Nanomedicine (CIBER-BBN) Campus UAB, 08193 Bellaterra, Spain*

3) *Consiglio Nazionale delle Ricerche (CNR)- Instituto per la Microelettronica e Microsistemi (IMM), 40129 Bologna, Italy*

4) *Institució Catalana de Recerca i Estudis Avançats (ICREA), 08193-Bellaterra, Spain*.

KEYWORDS

Hydro Resistivity, Quasi-two-dimensional Organic Metal, Humidity Sensor, Flexible Polycrystalline Nanocomposite, Sensing Mechanisms

ABSTRACT

With the emergence of environmental, biomedical and medical monitoring technologies, development of flexible and lightweight sensors is ongoing. This work presents a flexible lightweight bi-layer (BL) film (polycarbonate/polycrystalline layer of crystalline (BEDT-TTF)$_x$Br(H_2O)$_y$ salts [BEDT-TTF=bis (ethylendithio)tetrathiafulvalene]) as a promising material for humidity sensing which may be applied in a number of monitoring scenarios. X-ray structural characterization revealed the presence of three different crystal types in the crystalline layer of the BL film, *i.e.* [phase-I, [(BEDT-TTF)$_5$(Br_4(H_5O_2))]; phase-II, [(BEDT-TTF)$_2$Br(H_2O)$_3$]; and crystals of neutral BEDT-TTF compound] showing that phase-I is highly sensitive to humidity. The humidity testing of the BL film showed that it is capable of monitoring relative humidity (RH) levels from 15 up to 90% with a well-defined and reproducible electrical signal. Electrical resistance measurements revealed that the crystalline conducting layer is able to absorb moisture reaching equilibrium at constant RH as reflected in a stable relative resistance response. Structural response of the BL film to variations of RH clearly demonstrated that crystallite interlayer spacing (d) of phase-I is strongly affected exhibiting a reversible metal-non-metal transition, while phase-II was insensitive to humidity. Overview of mechanical and humidity sensing properties of the developed BL film corroborates that it can be used as flexible hygrometer as well as moisture sensing units on board of low-cost electronic sensing devices.

1) INTRODUCTION

Taking into account that manufacturing, storage and testing processes are humidity-critical, relative humidity (RH) is one of the most frequently controlled parameters in science and technology. More important aspects of moisture control are related to human health:[1] the key factor, which affects the development of fungi, viruses, and bacteria, is RH.[2] Suitable sensors for biomedical applications are challenging to make, since lightweight, flexibility and low-cost, while maintaining fast and fully reversible RH responses, are basic requirements. In this context, flexible nanocomposite films with polycrystalline layers of hydrated organic molecular conductors as active components may open a new avenue to address these issues.

The history of BEDT-TTF-based molecular conductors began back in 1984 [BEDT-TTF=bis(ethylenedithio)tetrathiafulvalene, **Scheme 1**], when the first quasi-two-dimensional organic superconductor β-(BEDT-TTF)$_2$I$_3$ was reported.[3]

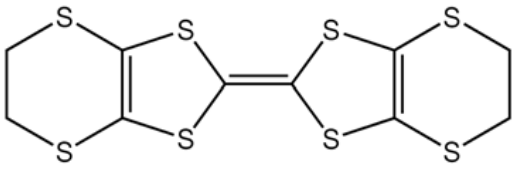

Scheme 1. Chemical structure of BEDT-TTF=bis(ethylenedithio)tetrathiafulvalene.

Soon it became clear that ion radical salts (IRSs) derived from BEDT-TTF exhibit modulable electronic band structures being, therefore, such molecules excellent building blocks for engineering a rich and diverse family of organic crystalline metals and semiconductors.[4-6] Electronic band structures of BEDT-TTF-based molecular conductors originate from ordered arrangements, such as stacks and layers, leading to metallic charge-transfer salts with partially

filled bands.[7-13] Over the years, many BEDT-TTF-based metals and semiconductors have been synthesized and basic electronic properties of quasi-two-dimensional conducting systems have been experimentally studied.[14-18] One interesting characteristic of BEDT-TTF-based crystalline conductors is the very deformable molecular and crystal structure with strong electron-electron and electron-phonon couplings. Thanks to this, their anisotropic electronic structures exhibit many fascinating electronic and structural phase transitions caused by lattice deformations, which can be controlled by external stimuli such as light, temperature, strain, pressure and, humidity among others.[19-28]

The high electrical resistance response of BEDT-TTF-based crystalline molecular conductors to external stimuli associated with crystal lattice deformations makes them ideal candidates for applications in sensing technologies. Recently, in a highly ambitious project such materials were also proposed as small band gap sensor materials for Dark Matter detection.[29] Nevertheless, it is necessary to engineer these crystals into a proper material for sensing applications. This was done by forming polycrystalline layers of IRSs, derived from BEDT-TTF-based conductors, in nanocomposite bi-layer (BL) films, a strategy that allows combining electrical properties of IRSs with classical properties of insulating polymers, like flexibility, transparency and processability.[30-33] Indeed, the high chemical tuneability of BEDT-TTF-based IRSs in combination with the structural and electronic modifications of these IRSs responsive to external inputs have allowed to date fabricating a variety of sensor elements for strain,[33] pressure,[34] temperature,[35] and IR radiation (bolometer)[36] sensors. However, the development of sensor elements for RH with these IRSs is less mature and only a few examples have been reported, without fully disentangling their sensing properties.[37-40]

State-of-the-art humidity sensors show us that, from a materials point of view they are often divided into three groups: organic polymers, electrolytes, and porous ceramics. As shown in extensive literature reviews, many different designs and device layouts have been reported.[41-42] Resistive type of sensors are typically found with an accuracy of about 3% RH. Calibrated capacitive humidity sensors, exhibit typically 2% of accuracy in the range from 5% to 90% RH. Optical hygrometers, measure absorption of light by water in air, and typically exhibit an accuracy of 0.5% to 1% RH.[41-43]

Important advances have been made in recent years especially for sensors with electrical readout, such as impedance[44] (or resistance[45]) and capacitance,[46] and are widely used in modern automatic control systems.[41-42] Carbon nanotubes, carbon fiber, and graphene are appealing for humidity sensors,[47-48] but exhibit often temperature dependent electrical signals, detrimental for selective RH sensing.[49] Unfortunately, many of the aforementioned sensor platforms reveal a lack in stability reflected in a decrease of signal reversibility and poor reliability in long-term operation.[47, 50] In this context, organic conductive materials hold great promise for the development of innovative sensors. For devices based on semiconducting polymers, it is known that the presence of water inside the active layer has substantial impact on their electrical response.[51-52] Swelling of one or multiple components in composites under the influence of external stimuli has a strong impact on charge transport properties as reported for instance in insulating polymers filled with metal nanoparticles able to exhibit an electrical transition from metallic conductors to insulators.[53]

The discovery of quasi-reversible modulation of electrical resistance depending on the RH in BL films composed of polycarbonate (PC) and hydrated molecular BEDT-TTF or BEDO-TTF [BEDO-TTF=bis(ethylenedioxy)tetrathiafulvalene] conductors[37-39] allows engineering a

new type of organic materials for the development of flexible humidity sensors. As already mentioned the origin of charge transport changes under the influence of different RH levels in both BL-films remains to be unraveled. So, even though it was previously hypothesized that RH has a substantial impact on the IRS crystal structures,[37-39] playing an important role in charge transport, no direct experimental evidence with a systematic characterization and understanding is available. Here we report a detailed study of the influence of RH on the resistive properties of BL films composed of PC and halogenated IRSs derived from BEDT-TTF. In particular we studied the structural and electronic properties in distinct humidity environments of BL films composed of a PC layer and a polycrystalline layer of two $(BEDT\text{-}TTF)_xBr(H_2O)_y$ salts (**F1**). For comparison purposes we also studied the electronic properties in distinct humid environments of BL films derived from IRSs without H_2O molecules in their structures: PC/α-$(BEDT\text{-}TTF)_2I_3$ (**F2**) and PC/β-$(BEDT\text{-}TTF)_2I_3$ (**F3**). The structural and electrical responses of the polycrystalline layer of **F1** to RH changes allow proposing a working mechanism of this hydro-resistive nanocomposite film sensor. Additionally, also the temperature dependence of resistance and the electromechanical properties of such a BL film were studied, suggesting the possibility of using **F1** as a flexible humidity sensor.

2) RESULT AND DISCUSSION

2.1) Preparation and structural characterization of BL films

We prepared representative BL-film samples comprising thin films of about 20 μm thickness of PC and a 2 μm thick top-layer of three conducting polycrystalline networks of IRSs: (**F1)** with $(BEDT\text{-}TTF)_xBr(H_2O)_y$ salts that has coordinating water molecules inside their structure and two other films with IRSs α-$(BEDT\text{-}TTF)_2I_3$ (**F2**) and β-$(BEDT\text{-}TTF)_2I_3$ (**F3**)

without water molecules in their crystal structures. These BL-films were prepared as previously reported[33] (see also Experimental Section and Supporting Information (SI)). We choose PC as the polymer support for the top polycrystalline IRS in the BL-films, because the water permeation coefficient of this polymer remains almost invariant in the RH range of 20% to 80% and at temperatures between 25º and 80ºC minimizing water changes inside the microenvironments of the nanocomposite.[54] Consequently, changes of electrical properties of BL-film induced by varying RH will originate from modification of the IRS properties rather than those of PC.

With the aim to unravel the sensing mechanism of BL-films, we first identified by X-ray diffraction the composition and crystal phases of as-formed IRS crystals during the preparation. As expected, X-ray diffraction patterns of **F2** and **F3** showed only high order reflections corresponding to (*00l*) oriented submicron sized crystals of the well-known organic molecular conductors α- and β-(BEDT-TTF)$_2$I$_3$, respectively (**Figure S2**).[33] At this orientation, the *c** axis of the linked network of submicron crystals is perpendicular to the film surface and, consequently, their conductive molecular BEDT-TTF-based layers are orientated parallel to it.

Figure 1a shows the X-ray diffraction pattern of **F1,** measured at T = 24 ± 3 ^{o}C and RH of 45 ± 5 %, which suggests a more complex structural composition. Indeed, the recorded diffraction peaks cannot be ascribed to a unique crystal phase and the coexistence of three different crystalline phases in the top-layer of BL **F1** has to be assumed. Two phases correspond to two different arrangements of hydrated BEDT-TTF bromide salts. The first one, called hereafter phase-I, [(BEDT-TTF)$_5$(Br$_4$(H$_5$O$_2$))] is a metal that contains a [Br$_4$(H$_5$O$_2$)]$^{3-}$ cluster for every five BEDT-TTF molecules,[55] where the four bromide ions are organized in an approximate square, bridged by hydrogen bonding to a [H$_2$O···H$^+$···OH$_2$] unit. Only the (*0k0*) peaks of this

phase are recorded in the XRD patterns of **F1**, indicating a pronounced texturing of the film. The slight difference between the experimental d_{010} value (17.05 ± 0.13 Å) and the corresponding value of the single crystal (16.61 Å)[55] may be explained either by assuming a slight different molecular arrangement in the film system (*thin film phase*) or to a higher humidity during **F1** measurements, since the interplanar spacing is highly sensitive to the RH (*vide infra*). The second hydrated phase, hereafter named phase-II, is a weak metal above 230 K identified by the *h00* family of reflections of the [(BEDT-TTF)$_2$Br(H_2O)$_3$] salt.[56] Also for this phase in **F1** only the presence of one family of planes indicates a pronounced texturing of the film with an interlayer spacing d_{200} =16.35 ± 0.06 Å, corresponding to the bulk one (16.4 Å). The texturing of both phases corresponds to the upright orientation of BEDT-TTF molecules sandwiched between anion layers, as reported previously for similar structures. Similar orientation was also reported for the conducting α-, β-(BEDT-TTF)$_2I_3$ polycrystalline layers.[33] Finally, a third phase corresponding to crystals of the neutral donor BEDT-TTF molecules was identified[57] by the *0kl* = 011 reflections. Neutral BEDT-TTF crystals are not able to participate in electrical charge transport, and are therefore not responsible for the changes observed in the electrical properties of **F1**. By collecting a 2D-GIXRD image it was possible to resolve the polycrystalline nature of **F1**, characterized by the co-presence of random oriented domains (rings in the 2D-GIXRD image, Figure 1b) and textured (arc shaped Bragg spots along the Q_z direction, **Figure 1c**). The disentangled three groups of **F1** reflections with corresponding crystal structures and their orientation on top of the PC-matrix with crystal axes are reported schematically in **Figure 1d**.

2.2) Electro-thermal and electro-mechanical characterizations of BL film F1

Hereafter the resistance of the conducting layer of the BL-films will be referred as resistance of **F1**, **F2** and **F3**. Since the primary readout parameter of BL-film based sensors is

electrical resistance that changes with temperature (pyro-resistivity),[36] we first measured the temperature response of resistance of **F1** at constant RH = 40 ± 5 %. **Figure 1e** shows a clear metallic temperature dependence of resistance measured in **F1** employing 4-probe-dc measurements in a temperature range of $28^{o}C < T < 80^{o}C$. An empirical expression, such as an expansion into *Taylor* series, is often used for sensor calibration and extraction of corresponding calibration coefficients.[58-59] Thus, the temperature dependence was modeled by the following expression: $R(T) = R_0 [100 + \xi'(T-T_0) + \xi''(T-T_0)^2]$; where ξ'(in %/K) and ξ''(in $\%/K^2$) are first and second order coefficients, respectively, exhibiting a good quality of fit: $R^2 = 0.9998$ and $R_0 = 177\ \Omega$ at $T_0 = 30.15 \pm 0.04\ ^{o}C$. First and second order temperature-resistance coefficients were found to be $\xi' = 0.184 \pm 0.001$ (%/K) and $\xi'' = (1.0 \pm 0.2)\cdot 10^{-3}$ ($\%/K^2$), respectively, and are well in agreement with previously reported data on single crystal of IRS derived from BEDT-TTF (phase-II).[56, 60] Such values also reflect an almost linear and weak metallic temperature dependence in the measured temperature range of **F1.** In contrast to that, for instance, the highly sensitive pyro-resistive material, α'-$(BEDT\text{-}TTF)_2I_xBr_{3-x}$ exhibits a high linear semiconducting temperature resistance coefficient of $\xi' = -1.27$ (%/K).[36] These findings are particularly important for the development of selective sensor systems, *i.e.* the decoupling of RH and temperature responses (*vide infra* and Section S4.1 of Supporting Information).

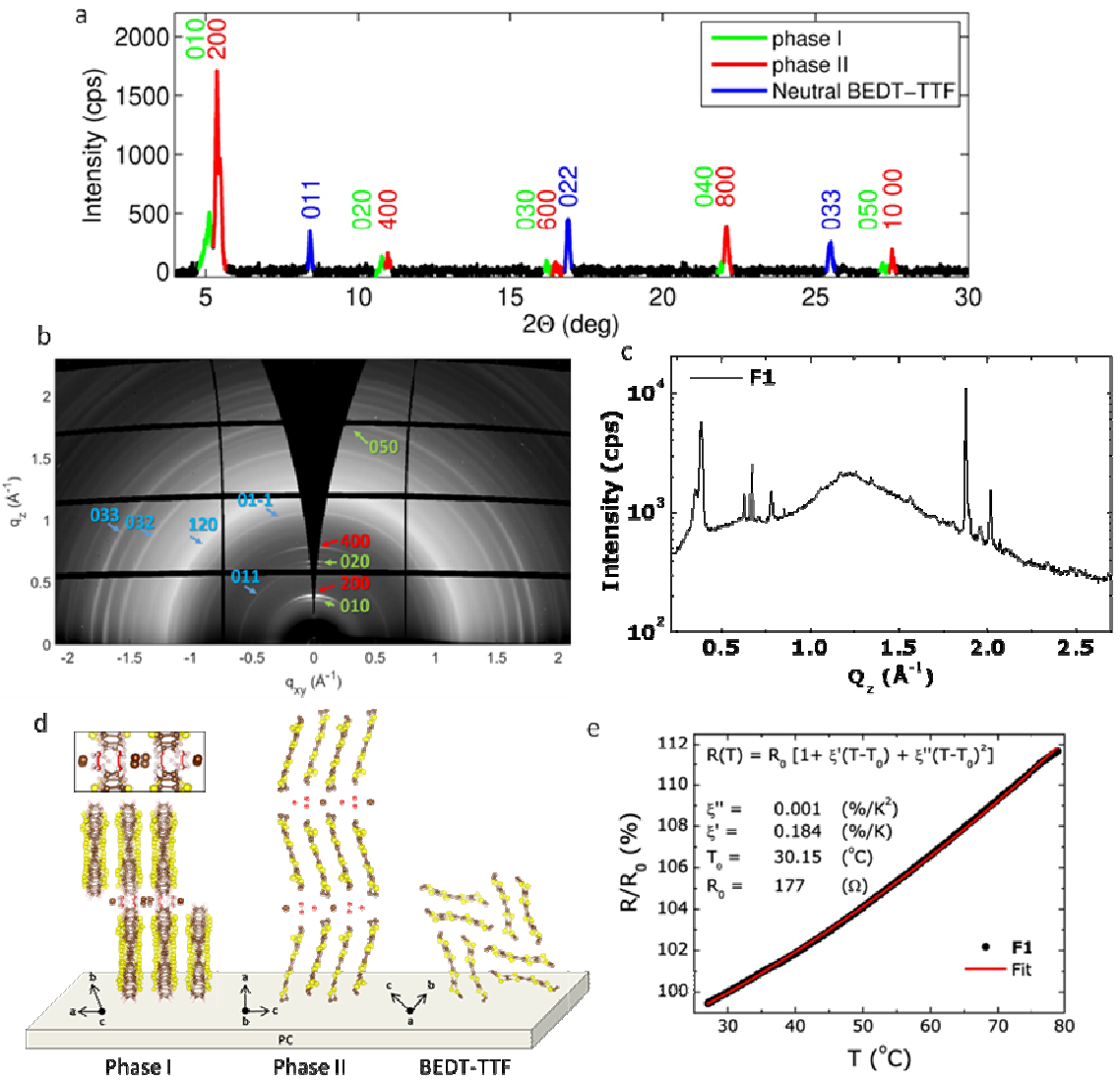

Figure 1. Structure and electro-thermal response for BL-Film F1. a) Specular X-ray diffraction pattern of composite BL-Film F1. b) 2D-GIXRD image of BL-film **F1**, c) extracted scan along Q_z. d) Schematic representation of BL-films comprising polycarbonate (PC) matrix with topmost polycrystalline network of the molecular metal [BEDT-TTF]$Br_x(H_2O)_y$ (**F1**) identifying crystal orientation of phase-I,[55] phase-II[56] and neutral BEDT-TTF.[57] C, S, H, Br and O atoms are grey, yellow, white, brown and red, respectively. Small inset shows $[Br_4(H_5O_2)]$ anion layer. e) Temperature dependence of resistance measured under ambient conditions employing 4-probe-dc technique in a range of 28^{o}C < T < 80^{o}C.

With the aim to unravel the electromechanical response of **F1,** stress-strain characteristics were recorded by measuring simultaneously the electrical resistance and uniaxial elongation, Δl. **Figure S4** shows the stress and relative electrical resistance change of **F1** with strain, ε, values [$\varepsilon=\Delta l/l_0 \cdot 100$; where l_0 is the initial length of the BL film] of up to ε = 2%. While the stress measured in **F1** shows clear sub-linear strain dependence, the relative resistance starts to increase super-linearly at high strain values. This in fact is not surprising as it reflects the elastic-plastic transition of the polymer matrix, a phenomenon well known in the field of polymers, and in agreement with previous measurements on full organic strain gauges.[33] The linear dependence of both stress and relative resistance at strain values below 0.6% strengthens the proposed hypothesis above. In the region of ε < 0.6% we calculate both the gauge-factor ($k(\varepsilon) = \partial[\Delta R/R_0]/\partial\varepsilon$) and the Young's modulus ($YM(\varepsilon) = \partial\sigma/\partial\varepsilon$), where σ is the uniaxial stress (in Pascals), **Figure S5**. A fairly constant gauge factor of about 9 ± 1 was found. Constant gauge factors of k=9.91±0.09 and k=18.4±0.3, for **F2** and **F3**, respectively, were found for strain below 0.6% (Table S2). For piezo-resistive BL-films with the same molecular donor, **F2** and **F3**, a clear contraction of the crystal d-spacing of up to $\Delta d/d_0$ = -0.05% and $\Delta d/d_0$ = -0.14%, respectively under uniaxial strain, (0 % < ε < 1 %) applied parallel to the film surface was previously shown.[33] This is in agreement with differences in softness of crystal structures, where the β-phase is much softer than the α-phase. On the other hand, the Young's modulus of **F1 (Figure S5)** extracted parallel to the film surface attains a constant value of about 1.27 ± 0.03 GPa, in accordance with values found for **F2** and **F3** (**Table S3**). It is worth mentioning that the Young's modulus in human tissues is found in a wide range spanning from 0.1 MPa up to 1 GPa, including organs, tissues and tissue components,[61] highlighting thus the mechanical compatibility of BL-films with biological tissues. In fact, BL-films derived from TTF-based IRSs exhibiting

high piezo-resistive response have previously been used in applications such as strain gauges[33] or pressure sensors.[34] This means that both electrical resistance and Young's modulus exhibit stable linear dependences on strain within the elastic and reversible regime of deformation. Both characteristics facilitate the engineering of films for electronic devices with biomedical applications.

2.3) Hydro-resistive characterizations of BL film F1

Aiming at humidity sensors, the resistance changes of **F1**, **F2** and **F3** were analyzed at various RH levels (**Figure 2a**). Measurements were carried out within a commercial humidity chamber that allows stabilizing temperature and RH. The resistance of **F1** monotonically increases with RH level, whereas electrical responses of **F2** and **F3** are almost independent on RH.

For all three types of BL-films the following empirical expression for resistance changes was used: $R(\phi) = R_0 [100 + \xi'(\phi-\phi_0) + \xi''(\phi-\phi_0)^2]$; where ξ' (in %/%RH) and ξ'' (in %/%RH^2) are first and second order coefficients, respectively, and ϕ (in %RH) corresponds to the RH level. As mentioned earlier, this approach is often used for sensor calibration and extraction of corresponding calibration coefficients, and is not limited to a specific type of sensor.[58-59] **Table 1a** gives a summary of coefficients extracted from good quality fits for **F1**, **F2** and **F3** at T = 25 ± 1^{o}C including standard errors. By analyzing the response of **F2** a second order coefficient close to zero ($\xi'' = 0$) and a very low first order coefficient of $\xi' = 0.004 \pm 0.001$ (in %/%RH) was found. On the other hand, for **F3** both first and second order coefficients have been found to be close to zero ($\xi' = \xi'' = 0$). These results mean that **F3** is not sensitive towards changes of RH

and **F2** shows a very low linear response. Moreover, this stays in agreement with the tight molecular packing of BEDT-TTF in the submicron crystals of BL-films **F2** and **F3**, and the absence of H_20 in their crystal structures.[62] On contrary, BL-film **F1** shows a completely different behavior since it exhibits a higher first coefficient (ξ' = 0.04 ± 0.03 (in %/%RH) and, most importantly, a much higher second order coefficient (ξ'' = 0.0027 ± 0.0007 (in %/%RH^2)) indicating that **F1** is highly sensitive to humidity.

Humidity sensors with electrical dc-resistance readout typically exhibit linear resistance-RH dependence, which has mostly been attributed to moisture sorption on the sensor surface.[43] The conducting layer of **F1** demonstrates stronger resistance-RH behavior compared to first order dependence (black trace in **Figure 2c**). This means that another mechanism rather than sorption of water on its surface is responsible for the resistance change. With the aim to unravel the working mechanisms of such sensor systems, both temperature and pressure were maintained constant during a humidity sweep. Additionally, the rate of humidity change was set to comparable values (**Figure S11**).

Resistance response of **F1** was measured with a commercial temperature controlled humidity chamber which allows stabilizing the RH between 10% and 90% at T = 25°C thanks to a small Peltier heater and continuous moisture supply. **Figure S7** shows a fast and fully reversible resistance response of **F1** to a RH change from 20% to 30 %, 40 % and 60 %. In addition, resistance stability of **F1** at constant RH levels at T=25°C was verified by measuring the electrical resistance in 4-wire configuration at RH equal to 20%, 40%, 60%, 80% and 90% **(**see **Figure 2b**). The same experiment also allowed extracting the response speed of **F1** *i.e.* the stabilization time of resistance after the RH level was changed. A stabilization time of about 10 ± 2 s was extracted for humidity steps of 20 % (RH from 20% to 40%, from 40% to 60%, from

60% to 80%) and of 10% (RH from 80% to 90%, **Figure S8**). The first derivative shows ripples after stabilization at all the chosen RH values. Moreover, the ripple amplitude increases with increasing RH (**Figure S9**). The frequency of the calculated time-derivative is the same of the humidity stabilization cycle of the Peltier-based humidifier, evidencing the extremely large sensitivity of **F1** to RH changes. The slightly lower response at RH= 90% was attributed to the limitation of the commercial chamber and is well in agreement with the controllable RH range specified by the manufacturer. Resistance, current and voltage ranges of such sensor elements are fully compatible with low-cost open source electronics. Selectivity and sensitivity to RH may be further enhanced by implementing smart compensation schemes, such as active and passive sensor elements in a Wheatstone bridge. Thus, such a device enables to measure directly RH values of ambient at any temperature because of this smart compensating scheme (for more information see SI **Figure S14**).

Since temperature affects the RH value as the vapor pressure of water depends exponentially on temperature of the environment,[63-64] we also studied the resistance-humidity response of **F1** at different temperatures using a more precise and controllable homemade humidity chamber. This chamber included a set of commercial sensors able to monitor humidity, temperature as well as the ambient pressure. Relative Humidity inside this chamber was decreased by fluxing dry Nitrogen or Argon and increased by injecting small water drops. For **F1** resistance changes at various RH levels including temperatures of 25^{o}, 27^{o}, 37^{o} and 46^{o}C were measured and all results are shown in **Figure 2c**. As clearly observable, almost the same relative resistance response was measured for all tested temperatures. Table 1 shows a summary of resistance-humidity coefficients extracted for samples measured at different temperatures.

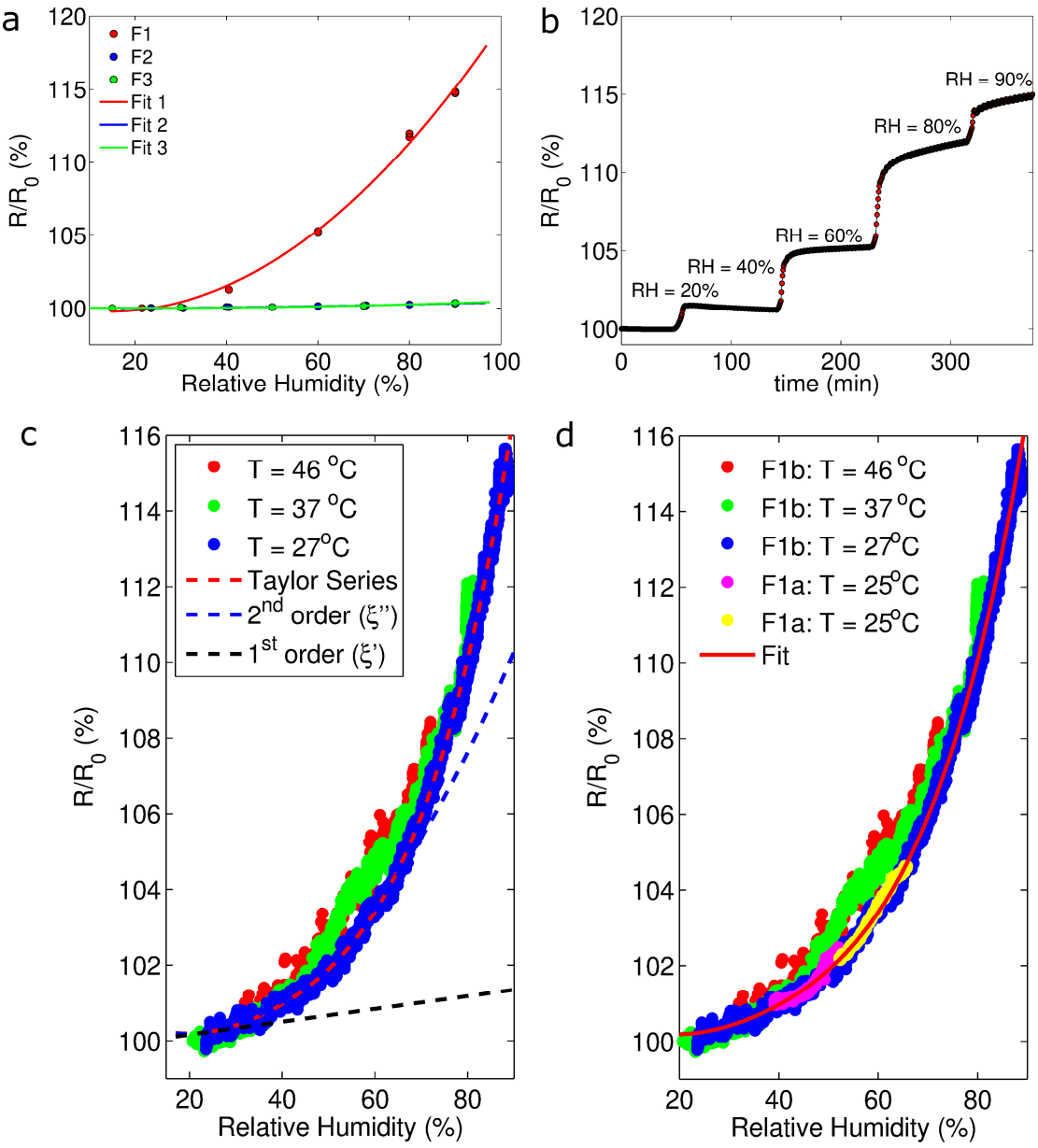

Figure 2. Humidity dependence of resistances for BL-films. a) Relative resistance changes of films **F1**, **F2** and **F3** exposed to different relative humidity ranging from 15 % to 90 %. b) Stability of relative resistance at different levels of humidity at T = 25°C. c) Relative resistance changes of **F1** exposed to different RH at temperatures of T = 27°, 37° and 46°C, shown in blue, green and red, respectively. Dashed lines in black, blue and red represent contributions of first (ξ'), second (ξ'') and higher order Taylor series regression, respectively. d) Relative resistance

changes of **F1** as function of RH shown for two samples (**F1a** and **F1b**) at different temperatures.

Table 1. Extracted fit parameters employing Taylor series as fit model. Resistance-humidity dependence of BL-films **F1**, **F2**, and **F3** with relative humidity ranging from 15 % to 90 % with ϕ_0=20%. ξ' and ξ'' are first and second order RH-resistance coefficients, respectively. R^2 represents the goodness of fit.

Humidity coefficients	BL-film **F1**	BL-film **F2**	BL-film **F3**
ξ' (in %/%RH)[a]	0.04 ± 0.03[a] (0.02 ± 0.01)[b]	0.004 ± 0.001[a]	0[a,c]
ξ'' (in %/%RH^2)[a]	0.0027 ± 0.0007[a] (0.0020 ± 0.0008)[b]	0[a,c]	0[a,c]
R^2	0.9967[a] (0.9974)[b]	0.9704[a]	0.9837[a]

a) Relative humidity coefficients obtained at 25C.
b) In parenthesis are the averaged relative humidity coefficients of Taylor series expansion for BL-film **F1a** and **F1b** obtained at temperatures ranging from T = 25, 27, 37 and 46^{o}C.
c) Standard error of fit higher than value of fit parameter; therefore assumption: ξ' = 0 and/or ξ'' = 0.

Two samples of **F1** measured under low relative humidity, *i.e.* RH < 5%, exhibited a pronounced increase in electrical resistance due to a different mechanisms (for more information see SI **Figure S13**). A total number of six different **F1** samples were studied under changing RH including: ambient air (about 400 ppm of CO_2, 21 % O_2 and 78 % N_2), 99% N_2 as well as 99% Ar. Sensitivity of **F1** in the range from 15% to 90 % was calculated to be about 95 Ω/%RH, 180 Ω/%RH, 335 Ω/%RH and 650 Ω/%RH for RH of 30%, 50%, 70% and 90%, respectively. Even though there was some variation in the initial resistance, sample-to-sample sensitivity variation was found to be within 5%. Signal linearization can be achieved by employing a logarithmic

amplifier (see Supporting Information **Figure S12**). Samples of **F1** stored under ambient conditions *i.e.* RH = 40 – 60 % and T = 15 – 30 ^{o}C, were found to be very durable with small variation in electrical resistance measured for a period of more than 10 years.

In summary, the electrical properties of BL-films **F2** and **F3** with no water molecules in their crystal structures were found to be (almost) independent of RH changes. In sharp contrast to that, the BL-film **F1**, which contains coordinating water molecules in its crystal structure, exhibited a clear super-linear electrical RH dependence; a signature of a high humidity sensitivity.

2.4) Mechanisms for humidity sensing of F1

With the aim to study the hydro-sensitive properties of **F1**, X-ray diffraction measurements at different humidity levels were done. This experiment was carried out by mounting **F1** in a small chamber suitable for X-ray measurements including the possibility to control and maintain stable RH. The structural change of **F1** film could be followed by monitoring the evolution of two diffracted peaks, *i.e.* the *010* of phase-I and the *200* of the phase-II (see **Figure 1d**). The RH was increased from 10% to 80% in steps of 10 %, and the system was kept at each RH value for about 1 h before recording the X-ray measurements in order to stabilize it. Temperature was measured and kept constant during the experiment exhibiting T = 23.4 ± 0.5 ^{o}C. **Figure 3** shows a series of XRD profiles of **F1** at different RHs. Upon increasing RH from 10% to 80% a shift of the *010* reflection of phase-I towards smaller diffraction angles is observed, corresponding to a vertical expansion of this lattice plane (**Figures 3a** and **3b**). On the other hand, it is not possible to detect any change of the *200* reflection of phase-II. The angular

shift of phase-I reflection was found to be fully reversible once the RH level was decreased again from RH of 80% to 10% (**Figures 3c** and **3d**). From these experiments we can conclude that the change of the level of RH to which **F1** is exposed results in a fully reversible structural change of crystals of phase-I, also called hereafter hydro-sensitive phase. Phase-II was not affected by altering RH and did not show any structural changes.

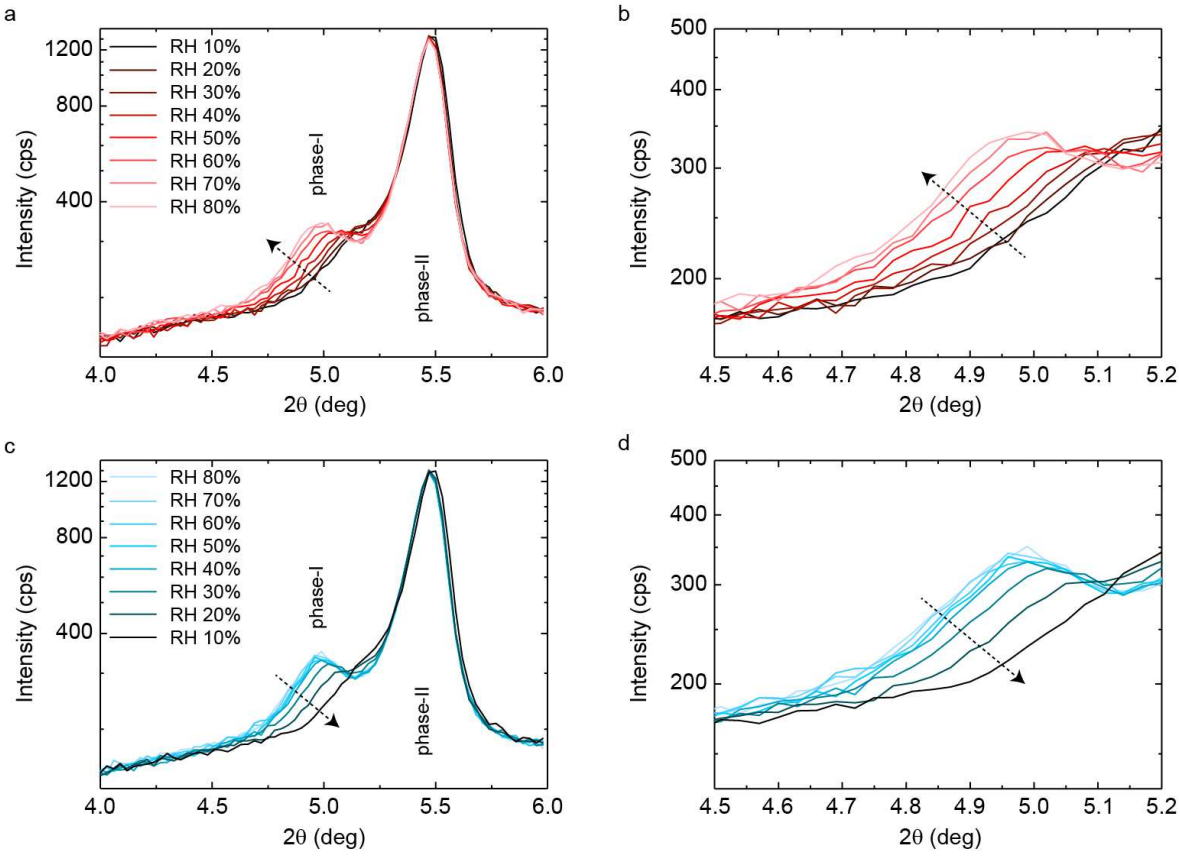

Figure 3. X-ray diffraction pattern at different relative humidity levels of BL-film F1. a) First reflections of phase-I and phase-II with relative humidity increase from RH = 10% to 80%, lasting for a total of 8 hours; b) magnification of phase-I changes. c), d) corresponding diffractions for decreasing relative humidity from RH = 80% – 10%. Arrows indicate shifts of the peak positions.

In order to correlate macroscopic electrical resistance response at different RH (**Figure 2**) with microscopic structural changes of **F1** obtained in X-ray measurements (**Figure 3**), relative *d*-spacing change, $\Delta d/d_0$, of the hydro-sensitive phase-I was calculated. Additionally, the coherence length was extracted from the peak width using the Scherrer equation. However, results exhibited high error preventing the study of their variation with relative humidity. **Figure 4a** shows $\Delta d/d_0$ for both increasing and decreasing RH demonstrating a fully reversible behavior exhibiting hysteresis. Boltzmann sigmoidal models have been successfully used to describe volume changes that occur during hydrophilic (swelling) and hydrophobic (collapsing) processes of gels,[65] or for temperature-induced structural phase transitions in self assembled networks.[66] We therefore used a Boltzmann sigmoidal to model $\Delta d/d_0$ at different RH (see Section S5 in SI for further details) exhibiting a good quality of fit with $R^2 = 0.997$ and 0.993 for RH increase and decrease, respectively. It was found that $\Delta d/d_0$ starts to increase slowly at low levels of RH, shows its highest RH dependence at about RH = 44 ± 1 % (corresponding slope = 0.19 ± 0.01) and stabilizes at high RH to a value of $\Delta d/d_0$ = 7.3 ± 0.2 %. The reverse RH change leads to similar stability $\Delta d/d_0$ values at low and high RH, but exhibits a much higher slope of 0.59 ± 0.01 at RH = 26 ± 1 %, leading to a total hysteresis of about 18 % in RH. It is interesting to notice that the lattice expansion, *i.e.* the d-spacing increment, happens gradually spanning from 10% to 80% of RH, whereas the inverse process occurs mostly between 30% and 20% of RH. This observation seems to indicate that, once embedded in the structure, water molecules are not easily released until a certain dry atmosphere is reached. Previously it has been shown that Br and Cl anions are stabilized with water molecules in many organic crystalline materials. For example, several conducting BEDT-TTF-based salts (*i.e.* BEDT-TTF = ET: $(ET)_5(Br_4(H_5O_2))$, $(ET)_4Cl_2(H_2O)_6$, $(ET)_4Cl_2(H_2O)_4$, $(ET)_3Cl_{2.5}(H_5O_2)$, $(ET)_3Cl_2(H_2O)_5$, $(ET)_3Cl_2(H_2O)_2$,

$(ET)_3Br_2(H_2O)_2$, $(ET)_2Br(H_2O)_3$) have been synthesized.[55, 67-68] In such systems, halogen ions and water molecules (or hydroxonium cations) are held together by hydrogen bonds.

Figure 4b shows the relative resistance response of **F1** to changes of RH at T = 27 ± 1°C analytically described by the following exponential expression: $R(\phi) = R_0\ [100 + \zeta \exp[\eta \cdot (\phi - \phi_0)]]$. R_0 = 280 ± 5 kΩ in this formula corresponds to the resistance at relative humidity level ϕ_0 = 20% and ζ = 0.68 ± 0.01% is a pre-exponential factor. The resistance response over RH variation was defined as η and found be about 4.87 ± 0.03 (in %/%RH) with a good quality of fit exhibiting R^2 = 0.997. A similar exponential dependence was previously attributed to a metal-insulator transition in insulating-polymer/metal-nanoparticle composites.[53]

By substituting RH with relative d-spacing it is possible to calculate changes of relative resistance as function of $\Delta d/d$, which is shown in **Figure 4c.** Two clear regimes have been identified: i) linear R/R_0 dependence at $\Delta d/d_0 < 4.5$ %, in agreement with a region where both $\Delta d/d_0$ and R/R_0 increase exponentially with RH; and ii) strong R/R_0 dependence at high $\Delta d/d_0 >$ 4.5 % with a limit value of $\Delta d/d_0$ =7.3 ± 0.2 %, in agreement with $\Delta d/d_0$ stabilization as predicted by the Boltzmann model. These two regimes have been successfully de-convoluted (see SI, Section S5). The initial linear increase may be attributed to an expanding crystal structure altering intermolecular distances in the polycrystalline film. On the contrary, to explain the second regime we have to consider that the conductive linked crystallites of BL-films exhibit sandwiched structures of their molecular conducting BEDT-TTF-based radical cation layers with insulating layers of the counter anion,[12] both orientated parallel to the film surface. The increasing of interlayer distance of the crystallites of the hydro-sensitive phase-I (*i.e.* increase in d-spacing), takes place just perpendicular to the charge transport plane.

According to classical percolation theory, a metal-non-metal transition takes place, when the volume fraction of the metallic phase approaches the percolation threshold.[69] Critical indexes describe the behavior of conductivity near the threshold as function $\sigma(x) = \sigma_0 \cdot (x-x_c)^t$ of the volume fraction, x, where x_c is the critical volume fraction and t the critical exponent.[70] The de-convoluted relative resistance change as function of relative d-spacing can be approximated with a similar model: $R/R_0 \approx b \cdot (x_c-x)^t$, with t =-1 and x_c = 7.3 ± 0.2 %, the critical exponent and critical d-spacing, respectively. This is in agreement with the hypothesis stated before, where an increase of the distance between the anion layer and BEDT-TTF molecules of the hydrosensitive phase-I affects the charge transfer integrals and, thus results in a metal-non-metal transition. We believe therefore that such high R/R_0 dependence could be described by variations in charge transfer between radical cation and anion layers. This results in changes of the electronic band structure and overlap of delocalized π-electrons, responsible for electronic transport.

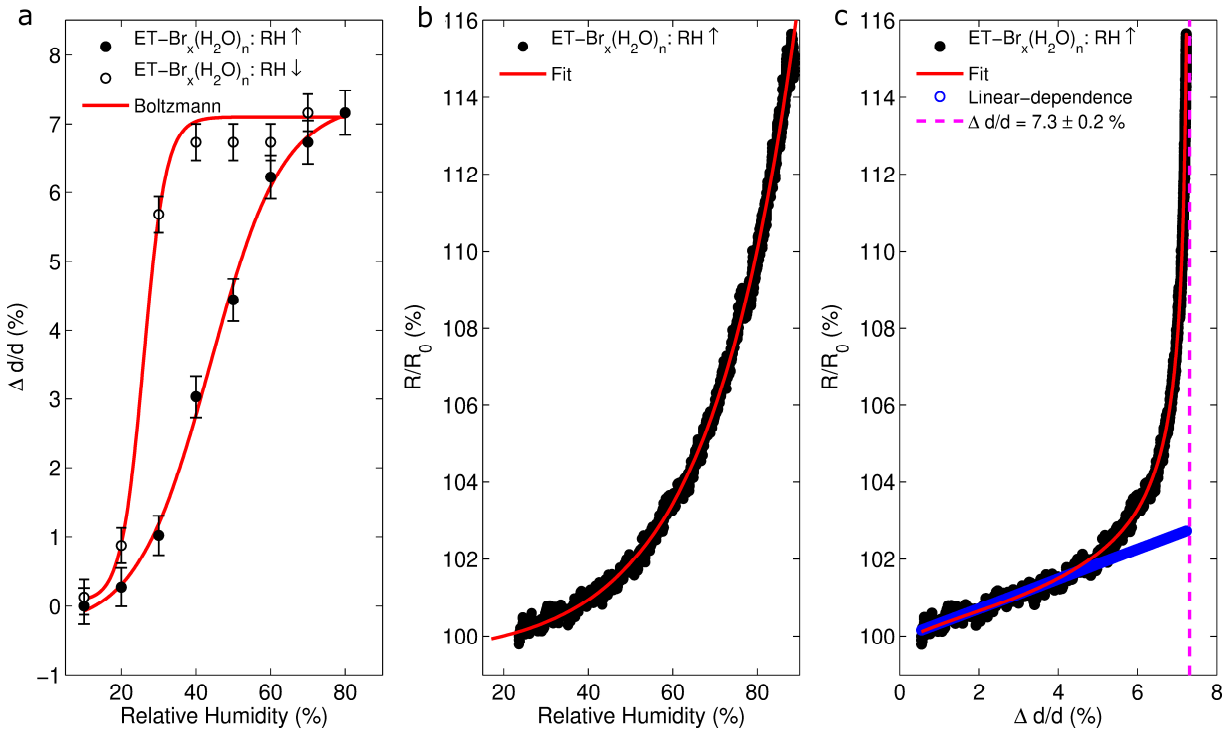

Figure 4. Correlation of changes in crystal structure and electrical resistance with relative humidity for F1. a) Relative d-spacing ($\Delta d/d_0$) of hydro-sensitive phase-I in F1 at RH ranging from 10% to 80%, fitted with Boltzmann's sigmoidal (see SI, Section S5 for further details). Error bars correspond to standard errors in Gaussian peak deconvolution, well within the resolution of XRD measurements. b) RH dependence of relative resistance (R/R_0) modeled with a first order exponential regression: $R/R_0 \approx \exp[\eta \cdot (\phi - \phi_0)]$. c) Relative d-spacing dependence of R/R_0 exhibiting two regimes: i) linear dependence for $\Delta d/d_0 < 4.5$ %, and ii) a strong R/R_0 increase for $\Delta d/d_0 > 4.5$ % asymptotically approaching a critical value of $\Delta d/d_0 = 7.3 \pm 0.2$ %.

3) CONCLUSION

The rich class of BL-films ranges from metallic, semimetal to semi-conducting charge transport and is highly sensitive to a variety of external stimuli. Appealing electronic properties of crystalline molecular conductors can be successfully transferred towards composites enabling processing qualities of polymers. Such materials allow for selective sensing enabled due to molecular design and structural control of the active components. BL-films exhibited fully reversible mostly linear response towards mechanical or thermal stimulation. A new highly hydro-sensitive nanocomposite BL-film, in agreement with a previously reported single crystal structure, able to swell under the influence of water exhibits a strong impact on the electrical resistance. Humidity uptake is translated into a fully reversible swelling of the composite exhibiting a relative change of resistance following a clear exponential dependence inducing the reversible metal-non-metal structural phase transition. Selective sensitivity to humidity may be further enhanced by implementing smart compensation schemes, such as active and passive sensors in a Wheatstone bridge. These findings are highly promising for multidimensional selective sensing made possible by tuning molecular composition to maximize and, importantly, to decouple responses to strain, pressure, temperature, radiation and recently also humidity as an external stimulus. An attractive field of application in this context is human health care, since for BL-film based devices the same temperature invariant humidity response was shown in temperature ranges relevant for human physiology.

4) MATERIALS AND METHODS

4.1) Materials and device preparation:

BL films preparation (see also SI): Bis(ethylenedithio)tetrathiafulvalene (BEDT-TTF), poly-(bisphenol-A-carbonate) (PC) in pellets (average Mw ca. 64,000) and 1,2-dichlorobenzene were purchased from Aldrich and used without further purification. PC films (20-25 μm thickness) with molecularly dispersed BEDT-TTF (typically 2 wt. %) were prepared by drop casting a solution of BEDT-TTF (0.02 g) and PC (0.98 g) in 1,2-dichlorobenzene (50 ml) on a glass surface within an oven at 130^{o}C. The sample was kept in the oven for 20 minutes for letting the solvent evaporate. A glass flask containing the binary system of the I_2/CH_2Cl_2 or Br_2/CH_2Cl_2 solution was enclosed in the chamber of a thermostat and left to equilibrate at 30^{o}C for 45 min. Subsequently, the samples were treated for 3 minutes with vapors of solvent and oxidant by placing them as a lid at the top of the flask. BL films **F1**, containing a polycrystalline layer of (BEDT-TTF)$Br_x(H_2O)_y$ salts, were prepared by exposing neutral films to vapors of Br_2 dissolved in CH_2Cl_2 (conc: = 0.5 - 10 mM) at T = 30 °C and a relative humidity of RH = 40 %. For **F2** preparation a saturated I_2/CH_2Cl_2 solution was employed. **F3** was prepared by heating **F2**, protected with a glass slide to avoid loss of iodine, at 150ºC for 15 minutes. The resulting BL films were fully characterized by scanning electron microscopy and X-ray diffraction.

4.2) Mechanical and electrical characterization, data analysis

Mechanical properties of BL-films were studied using a 5848 MicroTester, equipped with a 1 kg load cell (Instron). Film strips in dimension of about A = 28x2 mm^2, were held between two clamps positioned at a distance of about d = 18 mm. During measurement, the strips were pulled by the top clamp with velocity of about v = 2.0 μm/s. Both force (F) and elongation (ε) were monitored until sample rupture at high strain values. Measurements were carried out on two samples of **F1**, **F2** and **F3** BL-films.

The sensing capability to RH of BL film polycarbonate/polycrystalline (BEDT-TTF)$Br_x(H_2O)_y$ were studied in a climate chamber equipped with a Peltier element for automatic RH control working as a humidifier. (Memmert model HPP 108). RH in the climate chamber

was measured by a capacitive humidity sensor with an accuracy of 0.5 % and the temperature with a Pt100 sensor in 4-wire circuit with an accuracy of 0.1°C%. BL-Film samples with sizes of 8x8mm^2 were cut from the BL films and fixed with a very small amount of silicon grease on a copper substrate in order to eliminate temperature fluctuations during the measurements of resistance. Four graphite contacts were painted on each BL film and connected with 20 µm thick platinum wires to the measurement equipment capable to measure two samples simultaneously. A homemade humidity chamber including commercial sensors (BOSCH: BME280, combined humidity, temperature and pressure sensor; Aosong Electronics Co.Ltd DHT22, AM2302, capacitive-type humidity sensor and temperature sensor) for monitoring/controlling humidity, temperature and pressure was fabricated and is shown in Figure S10. If not otherwise stated, all electrical measurements were carried out using 4-wire dc-resistance measurements employing a constant current of I = 1 – 10 µA to prevent Joule heating. All remote measurements were carried out using homemade python measurement routines and data analysis was done with MATLAB.

4.3) Structural characterization

GI-XRD measurements were performed at the ELETTRA-XRD1 beamline at Trieste's synchrotron facility (Italy) using a monochromatic beam with a wavelength (λ) of 1 Å and a dimension of 0.2×0.2 (H×V) mm^2. The incident angle of the X-ray beam was chosen 0.1°, slightly larger than the critical angle for total reflection of the organic film, in order to penetrate through the full film depth. The diffraction pattern were recorded using a 2D camera (Pilatus detector) placed normal to the incident beam direction at 350 mm from the sample.

Specular XRD scans were performed using a SmartLab-Rigaku diffractometer equipped with a rotating anode (Cu Kα, λ = 1.54180 Å), followed by a parabolic mirror to collimate the incident beam, and a series of variable slits (placed before and after the sample position) The sample was mounted inside a box having two kapton windows to let pass the incident and diffracted beam through and a thermoigrometer to measure the RH and temperature in real time. RH was varied by changing the hydration of nitrogen flux inside the box. The flux rate was fixed to maintain the pressure constant.

ASSOCIATED CONTENT

Supporting Information. Additional information given in sections: S1) Preparation of BL-films. S2) X-Ray diffraction pattern of BL-film **F1, F2** and **F3** S3) Electromechanical characterization of BL-films and S4) Hydro-sensitivity of BL-Films **F1**. S5) Boltzmann's sigmoidal equation and de-convolution of relative resistance change. (file type PDF)

AUTHOR INFORMATION

Corresponding Authors

Dr. Raphael Pfattner*, Email address: *rpfattner@icmab.es*

Dr. Elena Laukhina*, Email address: *laukhina@icmab.es*

Prof. Jaume Veciana*, Email address: *vecianaj@icmab.es*.

†) Current Address: EPFL STI IBI-STI LNE Campus Biotech, CH-1202 Geneva, Switzerland

Author Contributions

The manuscript was written through contributions of all authors. All authors have given approval to the final version of the manuscript.

ACKNOWLEDGMENT

Authors are grateful for the financial support received from projects MOTHER (MAT2016-80826-R) and FANCY (CTQ2016-80030-R) granted by the DGI (Spain), GenCat (2017-SGR-918), financed by DGR (Catalunya), and the Spanish Ministry of Economy and Competitiveness, through the "Severo Ochoa" Programme for Centres of Excellence in R&D (SEV-2015-0496) and through the "Proyecto interdisciplinar de frontera", FIP-2018 HECTIC-PTM. This study has been also supported by the Networking Research Center on Bioengineering, Biomaterials and Nanomedicine (CIBER-BBN), an initiative funded by the VI National R&D&I Plan 2008-2011, Iniciativa Ingenio 2010, Consolider Program, CIBER Actions and financed by the Instituto de Salud Carlos III with assistance from the European Regional Development Fund. R.P.

acknowledges support from the Marie Skłodowska Curie Cofund, Beatriu de Pinós Fellowship (AGAUR - 2017 BP 00064). The authors would like to acknowledge Prof. Ryszard Jachowicz and Dr. Jerzy Weremczuk from Warsaw University of Technology for complementary XRD experiments, and Dr. Tommaso Salzillo (ICMAB) for fruitful crystallographic discussions.

ABBREVIATIONS

Bis(ethylenedithio)tetrathiafulvalene (BEDT-TTF), Ion Radical Salt (IRS), poly-(bisphenol-A-carbonate) (PC), bilayer (BL), Relative humidity (RH), Direct current (dc).

REFERENCES

(1) Kakitsuba, N. Current knowledge on the effects of humidity on physiological and psychological responses. *Journal of the Human-Environment System* **2018,** *20* (1), 1-10.

(2) Dannemiller, K. C.; Weschler, C. J.; Peccia, J. Fungal and bacterial growth in floor dust at elevated relative humidity levels. *Indoor Air* **2017,** *27* (2), 354-363.

(3) Yagubskii, E. B.; Shchegolev, I. F.; Laukhin, V. N.; Kononovich, P. A.; Kartsovnik, M. V.; Zvarykina, A. V.; Buravov, L. I. Normal-pressure superconductivity in an organic metal (BEDT-TTF)2I3 [bis (ethylene dithiolo) tetrathiof ulvalene triiodide]. *JETP Letters* **1984,** *39* (1), 12-16.

(4) Williams, J. M.; Ferraro, J. R.; Thorn, R. J.; Carlson, K. D.; Geiser, U.; Wang, H. H.; Kini, A. M.; Whangbo, M.-H. *Organic Superconductors (Including Fullerenes): Synthesis, Structure, Properties and Theory*, Prentice Hall: Englewood Cliffs, New Jersey, 1992.

(5) Commeau, B.; Geilhufe, R. M.; Fernando, G. W.; Balatsky, A. V. Structural and electronic properties of α -(BEDT-TTF)2I3, β-(BEDT-TTF)2I3, and κ-(BEDT-TTF)2X3 (X = I, F, Br, Cl) organic charge transfer salts. *Physical Review B* **2017,** *96* (12), 125135.

(6) Hassan, N.; Cunningham, S.; Mourigal, M.; Zhilyaeva, E. I.; Torunova, S. A.; Lyubovskaya, R. N.; Schlueter, J. A.; Drichko, N. Evidence for a quantum dipole liquid state in an organic quasi–two-dimensional material. *Science* **2018,** *360* (6393), 1101.

(7) Bender, K.; Hennig, I.; Schweitzer, D.; Dietz, K.; Endres, H.; Keller, H. J. Synthesis, Structure and Physical Properties of a Two-Dimensional Organic Metal, Di[bis(ethylenedithiolo)tetrathiofulvalene] triiodide, (BEDT-TTF)+ 2 I− 3. *Molecular Crystals and Liquid Crystals* **1984,** *108* (3-4), 359-371.

(8) Shibaeva, R. P.; Kaminskii, V. P.; Yagubskii, E. B. Crystal Structures of Organic Metals and Superconductors of (BEDT-TTP)-I System. *Molecular Crystals and Liquid Crystals* **1985,** *119* (1), 361-373.

(9) Kübler, J.; Weger, M.; Sommers, C. B. Self-consistent band structure for β-(BEDTTTF) 2I 3. *Solid State Communications* **1987,** *62* (12), 801-805.

(10) Söderholm, S.; Girard, R. T.; Schweitzer, D. Electronic structure of the organic conductor α-(BEDT-TTF)2I3 studied by angle-resolvedand core-level photoelectron spectroscopy. *Physical Review B* **1997,** *55* (7), 4267-4274.

(11) Tajima, N.; Tamura, M.; Nishio, Y.; Kajita, K.; Iye, Y. Transport Property of an Organic Conductor α-(BEDT-TTF) 2I 3 under High Pressure - Discovery of a Novel Type of Conductor. *Journal of the Physical Society of Japan* **2000,** *69* (2), 543-551.

(12) Kondo, R.; Kagoshima, S.; Tajima, N.; Kato, R. Crystal and Electronic Structures of the Quasi-Two-Dimensional Organic Conductor α-(BEDT-TTF)2I3 and Its Selenium Analogue α-(BEDT-TSeF)2I3 under Hydrostatic Pressure at Room Temperature. *Journal of the Physical Society of Japan* **2009,** *78* (11), 114714.

(13) Kobayashi, A.; Katayama, S.; Suzumura, Y. Theoretical study of the zero-gap organic conductor α-(BEDT-TTF)2I3. *Science and Technology of Advanced Materials* **2009,** *10* (2), 024309.

(14) Williams, J. M.; Emge, T. J.; Wang, H. H.; Beno, M. A.; Copps, P. T.; Hall, L. N.; Carlson, K. D.; Crabtree, G. W. Synthetic Metals based on Bis(ethylenedithio)Tetrathiafulvalene (BEDT-TTF) - Synthesis, Structure, and Ambient-Pressure Superconductivity in (BEDT-TTF)2I3. *Inorg. Chem.* **1984,** *23* (17), 2558-2560.

(15) Jerome, D. Organic conductors: From charge density wave TTF-TCNQ to superconducting (TMTSF)(2)PF6. *Chemical Reviews* **2004,** *104* (11), 5565-5591.
(16) Shibaeva, R. P.; Yagubskii, E. B. Molecular conductors and superconductors based on trihalides of BEDT-TTF and some of its analogues. *Chemical Reviews* **2004,** *104* (11), 5347-5378.
(17) Kondo, R.; Higa, M.; Kagoshima, S.; Hoshino, H.; Mori, T.; Mori, H. Electrical and structural properties of theta-type BEDT-TTF organic conductors under uniaxial strain. *Journal of the Physical Society of Japan* **2006,** *75* (4), 044716.
(18) Saito, G.; Yoshida, Y. Development of conductive organic molecular assemblies: Organic metals, superconductors, and exotic functional materials. *Bulletin of the Chemical Society of Japan* **2007,** *80* (1), 1-137.
(19) Kartsovnik, M. V.; Kononovich, P. A.; Laukhin, V. N.; Khomenko, A. G.; Shchegolev, I. F. Investigation of the phase T-P diagram for α-(BEDT-TTF)2I3. *Zhurnal Eksperimentalnoi Teor. Fiz.* **1985,** *88* (4), 1447-1451.
(20) Laukhin, V. N.; Kostyuchenko, E. E.; Sushko, Y. V.; Shchegolev, I. F.; Yagubskii, E. B. Effect of pressure on the superconductivity of β-(BEDT-TTF)2I3 *Jetp Letters* **1985,** *41* (2), 81-84.
(21) Schwenk, H.; Gross, F.; Heidmann, C. P.; Andres, K.; Schweitzer, D.; Keller, H. α-(BEDT-TTF)2I3 and β-(BEDT-TTF)2I3 - 2 modifications with contrasting ground-state properties - insulator and volume superconductor. *Molecular Crystals and Liquid Crystals* **1985,** *119* (1-4), 329-335.
(22) Hardwick, D. A. The mechanical-properties of thin-films - A review. *Thin Solid Films* **1987,** *154* (1-2), 109-124.
(23) Saito, G.; Urayama, H.; Yamochi, H.; Oshima, K. Chemical and physical properties of a new ambient pressure organic superconductor with Tc higher than 10K. *Synthetic Metals* **1988,** *27* (1–2), A331-A340.
(24) Kund, M.; Veith, H.; Müller, H.; Andres, K.; Saito, G. Anisotropic uniaxial-stress dependence of the superconducting transition temperature in single crystals of κ-(BEDT-TTF)2Cu[N(CN)2]Br. *Physica C: Superconductivity* **1994,** *221* (1–2), 119-124.
(25) Maesato, M.; Kaga, Y.; Kondo, R.; Kagoshima, S. Uniaxial strain method for soft crystals: Application to the control of the electronic properties of organic conductors. *Review of Scientific Instruments* **2000,** *71* (1), 176.
(26) Maesato, M.; Kaga, Y.; Kondo, R.; Kagoshima, S. Control of electronic properties of α-(BEDT-TTF)2MHg(SCN)4 (M=K, NH4) by the uniaxial strain method. *Physical Review B* **2001,** *64* (15).
(27) Tamura, I.; Kobayashi, H.; Kobayashi, A. X-ray diffraction study of α-(BEDT-TTF)2I3 single crystal under high pressure. *Journal of Physics and Chemistry of Solids* **2002,** *63* (6–8), 1255-1257.
(28) Iwai, S.; Yamamoto, K.; Hiramatsu, F.; Nakaya, H.; Kawakami, Y.; Yakushi, K. Hydrostatic pressure effect on photoinduced insulator-to-metal transition in the layered organic salt α-(BEDT-TTF)2I3. *Physical Review B* **2008,** *77* (12), 125131.
(29) Geilhufe, R. M.; Olsthoorn, B.; Ferella, A. D.; Koski, T.; Kahlhoefer, F.; Conrad, J.; Balatsky, A. V. Materials Informatics for Dark Matter Detection. *physica status solidi (RRL) – Rapid Research Letters* **2018,** *12* (11), 1800293.
(30) Jeszka, J. K.; Ulański, J.; Kryszewski, M. Conductive polymer: reticulate doping with charge-transfer complex. *Nature* **1981,** *289* (5796), 390-391.

(31) Laukhina, E.; Tkacheva, V.; Shibaeva, R.; Khasanov, S.; Rovira, C.; Veciana, J.; Vidal-Gancedo, J.; Tracz, A.; Jeszka, J. K.; Sroczynska, A.; Wojciechowski, R.; Ulanski, J.; Laukhin, V. New conducting molecular metal/polycarbonate bilayered composites: (ET)2IBr2/PC-, (BET)2IBr2/PC- and (BET)2I3/PC-films. *Synthetic Metals* **1999,** *102* (1), 1785-1786.
(32) Mas-Torrent, M.; Laukhina, E.; Rovira, C.; Veciana, J.; Tkacheva, V.; Zorina, L.; Khasanov, S. New Transparent Metal-like Bilayer Composite Films with Highly Conducting Layers of θ-(BET-TTF)2Br·3H2O Nanocrystals. *Advanced Functional Materials* **2001,** *11* (4), 299-303.
(33) Laukhina, E.; Pfattner, R.; Ferreras Lourdes, R.; Galli, S.; Mas-Torrent, M.; Masciocchi, N.; Laukhin, V.; Rovira, C.; Veciana, J. Ultrasensitive Piezoresistive All-Organic Flexible Thin Films. *Advanced Materials* **2009,** *22* (9), 977-981.
(34) Sánchez, I.; Laukhin, V.; Moya, A.; Martin, R.; Ussa, F.; Laukhina, E.; Guimera, A.; Villa, R.; Rovira, C.; Aguiló, J.; Veciana, J.; Pastor, J. C. Prototype of a Nanostructured Sensing Contact Lens for Noninvasive Intraocular Pressure Monitoring. *Investigative Ophthalmology & Visual Science* **2011,** *52* (11), 8310-8315.
(35) Lebedev, V.; Laukhina, E.; Laukhin, V.; Somov, A.; Baranov, A. M.; Rovira, C.; Veciana, J. Investigation of sensing capabilities of organic bi-layer thermistor in wearable e-textile and wireless sensing devices. *Organic Electronics* **2017,** *42*, 146-152.
(36) Pfattner, R.; Lebedev, V.; Laukhina, E.; Kumar Suddapalli, C.; Esteban-Martin, A.; Ramaiah-Badarla, V.; Ebrahim-Zadeh, M.; de Arquer Pelayo García, F.; Konstantatos, G.; Laukhin, V.; Rovira, C.; Veciana, J. A Highly Sensitive Pyroresistive All-Organic Infrared Bolometer. *Advanced Electronic Materials* **2015,** *1* (8), 1500090.
(37) Haneda, T.; Tracz, A.; Saito, G.; Yamochi, H. Continuous and discontinuous water release/intake of (BEDO-TTF)2Br(H2O)3 micro-crystals embedded in polymer film. *Journal of Materials Chemistry* **2011,** *21* (5), 1621-1626.
(38) Yamochi, H.; Haneda, T.; Tracz, A.; Saito, G. Humidity dependent properties of a transparent conducting film doped with BEDO-TTF complex. *physica status solidi (b)* **2012,** *249* (5), 1012-1016.
(39) Lebedev, V.; Laukhina, E.; Rovira, C.; Laukhin, V.; Veciana, J. All-Organic Humidity Sensing Films with Electrical Detection Principle Suitable to Biomedical Applications. *Procedia Engineering* **2012,** *47*, 603-606.
(40) Steven, E.; Lebedev, V.; Laukhina, E.; Rovira, C.; Laukhin, V.; Brooks, J. S.; Veciana, J. Silk/molecular conductor bilayer thin-films: properties and sensing functions. *Materials Horizons* **2014,** *1* (5), 522-528.
(41) Yamazoe, N.; Shimizu, Y. Humidity sensors: Principles and applications. *Sensors and Actuators* **1986,** *10* (3), 379-398.
(42) Farahani, H.; Wagiran, R.; Hamidon, M. Humidity Sensors Principle, Mechanism, and Fabrication Technologies: A Comprehensive Review. *Sensors* **2014,** *14* (5), 7881.
(43) Fraden, J. *Handbook of Modern Sensors, Physics, Design and Applications*, Springer, New York: 2003.
(44) Tsuchitani, S.; Sugawara, T.; Kinjo, N.; Ohara, S.; Tsunoda, T. A Humidity Sensor Using Ionic Copolymer and its Application to a Humidity Temperature Sensor Module. *Sensors and Actuators* **1988,** *15* (4), 375-386.
(45) Mukode, S.; Futata, H. A semiconductive Humidity Sensor. *Sensors and Actuators* **1989,** *16* (1-2), 1-11.

(46) Molina-Lopez, F.; Briand, D.; de Rooij, N. F. All additive inkjet printed humidity sensors on plastic substrate. *Sensors and Actuators B: Chemical* **2012,** *166-167*, 212-222.
(47) Mogera, U.; Sagade, A. A.; George, S. J.; Kulkarni, G. U. Ultrafast response humidity sensor using supramolecular nanofibre and its application in monitoring breath humidity and flow. *Scientific Reports* **2014,** *4*, 4103.
(48) Qadir, A.; Sun, Y. W.; Liu, W.; Oppenheimer, P. G.; Xu, Y.; Humphreys, C. J.; Dunstan, D. J. Effect of humidity on the interlayer interaction of bilayer graphene. *Physical Review B* **2019,** *99* (4), 045402.
(49) Santra, S.; Hu, G.; Howe, R. C. T.; De Luca, A.; Ali, S. Z.; Udrea, F.; Gardner, J. W.; Ray, S. K.; Guha, P. K.; Hasan, T. CMOS integration of inkjet-printed graphene for humidity sensing. *Scientific Reports* **2015,** *5*, 17374.
(50) Guo, Y.; Yu, G.; Liu, Y. Functional Organic Field-Effect Transistors. *Advanced Materials* **2010,** *22* (40), 4427-4447.
(51) Nikolka, M.; Nasrallah, I.; Rose, B.; Ravva, M. K.; Broch, K.; Sadhanala, A.; Harkin, D.; Charmet, J.; Hurhangee, M.; Brown, A.; Illig, S.; Too, P.; Jongman, J.; McCulloch, I.; Bredas, J.-L.; Sirringhaus, H. High operational and environmental stability of high-mobility conjugated polymer field-effect transistors through the use of molecular additives. *Nature Materials* **2016,** *16*, 356.
(52) Nikolka, M.; Schweicher, G.; Armitage, J.; Nasrallah, I.; Jellett, C.; Guo, Z.; Hurhangee, M.; Sadhanala, A.; McCulloch, I.; Nielsen, C. B.; Sirringhaus, H. Performance Improvements in Conjugated Polymer Devices by Removal of Water-Induced Traps. *Advanced Materials* **2018,** *30* (36), 1801874.
(53) Chen, Z.; Pfattner, R.; Bao, Z. Characterization and Understanding of Thermoresponsive Polymer Composites Based on Spiky Nanostructured Fillers. *Advanced Electronic Materials* **2017,** *3* (1), 1600397.
(54) Moon, S. I.; Extrand, C. W. Water Vapor Permeation Resistance of Polycarbonate at Various Temperatures. *Industrial & Engineering Chemistry Research* **2009,** *48* (19), 8961-8965.
(55) Brooks, A. C.; Martin, L.; Day, P.; Lopes, E. B.; Almeida, M.; Kikuchi, K.; Fujita, W.; Sasamori, K.; Aktusu, H.; Wallis, J. D. Hydrogen bonded anion ribbons, networks and clusters and sulfur–anion interactions in novel radical cation salts of BEDT-TTF with sulfamate, pentaborate and bromide. *Dalton Transactions* **2013,** *42* (18), 6645-6654.
(56) Zhang, Q.; Wu, P.; Li, Y.; Zhu, D. Synthesis, structure and physical properties of ET2Br· 3H2O. *Synthetic Metals* **1998,** *98* (2), 129-133.
(57) Kobayashi, H.; Kobayashi, A.; Sasaki, Y.; Saito, G.; Inokuchi, H. The Crystal and Molecular Structures of Bis(ethylenedithio)tetrathiafulvalene. *Bulletin of the Chemical Society of Japan* **1986,** *59* (1), 301-302.
(58) Scaramuzza, D.; Martinelli, A.; Siegwart, R. In *A Toolbox for Easily Calibrating Omnidirectional Cameras*, 2006 IEEE/RSJ International Conference on Intelligent Robots and Systems, 9-15 Oct. 2006; 2006; pp 5695-5701.
(59) Na, Y.; Lanmei, W.; Taoli, W.; Ying-zeng, Y. In *Taylor series approximation for estimation of vector sensor array misorientation*, Proceedings of the 9th International Symposium on Antennas, Propagation and EM Theory, Nov. 29 2010-Dec. 2 2010; 2010; pp 1224-1226.
(60) Luo, M.; Ishida, T.; Kobayashi, A.; Nogami, T. Electrical conductivities and crystal and band-electronic structures of a new phase of BEDT—TTF—bromide salt, (BEDT—TTF)2Br(H2O)3. *Synthetic Metals* **1998,** *96* (2), 97-102.

(61) Akhtar, R.; Sherratt, M. J.; Cruickshank, J. K.; Derby, B. Characterizing the elastic properties of tissues. *Materials Today* **2011,** *14* (3), 96-105.
(62) Müller, H.; Svensson, S. O.; Fitch Andrew, N.; Lorenzen, M.; Xenikos Dimitrios, G. βco-(ET)2I3: Non-electrochemical synthesis and structural and physical properties of an organic superconductor with 7.1 K ≤ Tc ≤ 7.9 K. *Advanced Materials* **1997,** *9* (11), 896-900.
(63) Wexler, A. Vapor pressure formulation for water in range 0 to 100°C. A revision. *Journal of Research of the National Bureau of Standards - A Physics and Chemistry* **1976,** *80A* (Nos.5-6), 775-785.
(64) Flatau, P. J.; Walko, R. L.; Cotton, W. R. Polynomial Fits to Saturation Vapor Pressure. *Journal of Applied Meteorology* **1992,** *31* (12), 1507-1513.
(65) Navarro-Verdugo, A. L.; Goycoolea, F. M.; Romero-Meléndez, G.; Higuera-Ciapara, I.; Argüelles-Monal, W. A modified Boltzmann sigmoidal model for the phase transition of smart gels. *Soft Matter* **2011,** *7* (12), 5847-5853.
(66) Blunt, M. O.; Adisoejoso, J.; Tahara, K.; Katayama, K.; Van der Auweraer, M.; Tobe, Y.; De Feyter, S. Temperature-Induced Structural Phase Transitions in a Two-Dimensional Self-Assembled Network. *Journal of the American Chemical Society* **2013,** *135* (32), 12068-12075.
(67) Tracz, A. Ion exchange in (BO)2.4I3 microcrystals: A method for obtaining colorless, transparent, metallically conductive polymer films. *Journal of Applied Polymer Science* **2002,** *86* (6), 1465-1472.
(68) Hiraoka, K.; Mizuse, S.; Yamabe, S. Solvation of halide ions with water and acetonitrile in the gas phase. *The Journal of Physical Chemistry* **1988,** *92* (13), 3943-3952.
(69) Pope, M.; Swenberg, C. E. *Electronic Processes in Organic Crystals and Polymers*, 2nd ed.; Oxford University Press: Oxford, 1999.
(70) Efros, A. L.; Shklovskii, B. I. Critical Behaviour of Conductivity and Dielectric Constant near the Metal-Non-Metal Transition Threshold. *physica status solidi (b)* **1976,** *76* (2), 475-485.

TOC

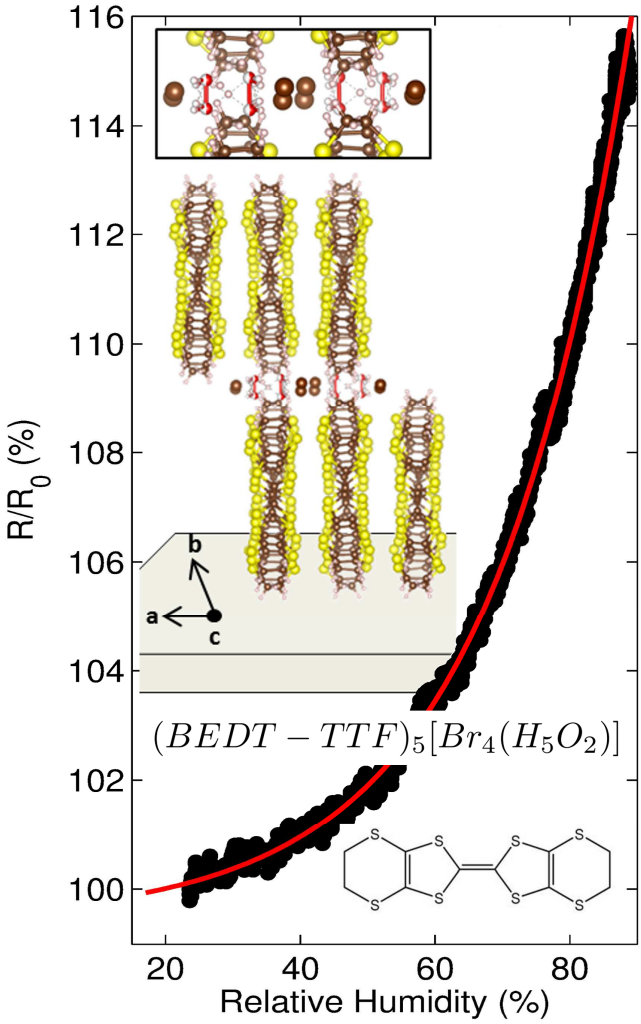
116
114
112
110
108
106
104
102
100
R/R0 (%)
20
40
60
80
Relative Humidity (%)
b
a
c
(BEDT − TTF)5[Br4(H5O2)]